ADVANCED MATERIALS
www.advmat.de

A Resistive Memory in Semiconducting $BiFeO_3$ Thin-Film Capacitors

An Quan Jiang, Can Wang, Kui Juan Jin, Xiao Bing Liu, James F. Scott,* Cheol Seong Hwang,* Ting Ao Tang, Hui Bin Lu, and Guo Zhen Yang*

Ferroelectric capacitive memories have not achieved the commercial success originally hoped for them in large volume because the area of the capacitors ("footprint") is too large to scale them up to gigabit density devices,[1] and a restoring pulse is required after a destructive readout. The non-destructive readout of the binary information is possible from the bipolar switching between high- and low-conductance of a ferroelectric diode under two opposite polarizations, as first discovered by Blom et al. in $PbTiO_3$ perovskite thin films[2] and later reported by Choi et al. in bulk $BiFeO_3$ single crystals and $Pb(Zr,Ti)O_3$ films.[3–5] Important properties of such memory are the ultrafast operating speed depending on the polarization flipping time (1–2 ps in principle)[6] and the high ratio of resistance in the forward and reverse directions (3000:1).[7] However, most ferroelectrics are insulating wide bandgap semiconductors at room temperature, which limits the maximum diode current to the order of ≈20 mA cm^{-2}.[2,3] Therefore, reaching a sufficient ferroresistive diode current for the stable detection of memory status using the sense amplifiers in modern memory circuitry with tiny cell size is a major challenge.

In such strongly insulating ferroelectrics, sufficient diode currents can, in fact, only be observed in ultrathin films, where quantum mechanical tunneling current dominates[8] and is modulated by varying the tunneling barrier height along with the polarization reversal. Although this effect has been reproducibly demonstrated through local electron transport from an atomic force microscope (AFM) tip into ferroelectric thin films,[9–11] the local-probe-based data storage is incompatible with current complementary metal-oxide semiconductor integration processes. Meanwhile, with macroscopic capacitor-type upper and lower electrodes capping the ultrathin ferroelectric layer, an overwhelming leakage current through existing defect-mediated leakage paths could swamp the tunneling current, thereby making the switching signal unreadable. In addition, large lattice-mismatch stresses in ultrathin epitaxial films prevent their use as longtime retention memories due to preferred domain orientations.[12]

One solution to these difficulties has been to more broadly consider resistive switching effects in (non-ferroelectric) metal oxides.[13–17] However, most of these resistive switching effects are based on a certain type of defect (ionic or electronic) mediated phenomenon, suggesting the inherent difficulty in precise control of the switching behavior. In contrast, ferroresistive switching behavior is based on the intrinsic switching of ferroelectric domains without invoking of charged defect migration and may, therefore, possess a fundamental merit over defect-mediated mechanisms for achieving reliable performance requisite for commercial production once reliable fabrication parameters are established. A critical measure of such success using ferroelectric semiconductors requires a physical understanding of the interplay between polarization and conduction and a viable technique to measure polarization–voltage (P–V) hysteresis loops. Note that prior work strictly avoided conductive ferroelectrics, requiring highly insulating capacitors.

720 semiconducting $BiFeO_3$ (BFO) thin films (24 runs of 30 @) with primary order parameters of antiferromagnetism and ferroelectricity[18] were deposited on (100) $SrTiO_3$ single-crystal substrates with epitaxial $SrRuO_3$ (SRO) lower electrodes using pulsed laser deposition; all showed diode behavior. Three different families of films, deposited at flowing O_2 pressures of 10, 10, 10, and 30 Pa with laser fluences of 1.5, 1.0, 1.0, and 1.0 J cm^{-2}, were denoted by BFO1, BFO2–1, BFO2–2, and BFO3, respectively (see the Experimental Section), and had thicknesses of 500, 240, 120, and 270 nm. Comparison of current behavior between BFO1 and BFO2–1/BFO2–2 tests the effects of thickness and comparison between BFO2–1/BFO2–2 and BFO3 tests effects of film growth mode. Out-of-plane film orientations were (001) and the films possessed rhombohedral distortion along one of four (111) crystallographic directions of the pseudocubic perovskite unit cell,[19,20] as determined from transmission electron microscopy and X-ray diffraction patterns (Supporting Information Figure S1a–d).

Under a poling pulse of +18 V (5 μs width) on BFO1 (all voltages were applied on the upper electrode while the

Prof. A. Q. Jiang, X. B. Liu, T. A. Tang
State Key Laboratory of ASIC & System
Department of Microelectronics
Fudan University
Shanghai, 200433, China
E-mail: jfs32@hermes.cam.ac.uk
Dr. C. Wang, Prof. K. J. Jin, Prof. H. B. Lu, Prof. G. Z. Yang
Institute of Physics
Chinese Academy of Sciences
Beijing 100190, China
Prof. J. F. Scott
Department of Physics
University of Cambridge
Cambridge CB3 0HE, UK
E-mail: jfs32@hermes.cam.ac.uk
Prof. C. S. Hwang
Department of Materials Science and Engineering and
Inter-university Semiconductor Research Center
Seoul National University
Seoul, 151–744, Korea
E-mail: cheolsh@snu.ac.kr

DOI: 10.1002/adma.201004317

© 2011 WILEY-VCH Verlag GmbH & Co. KGaA, Weinheim

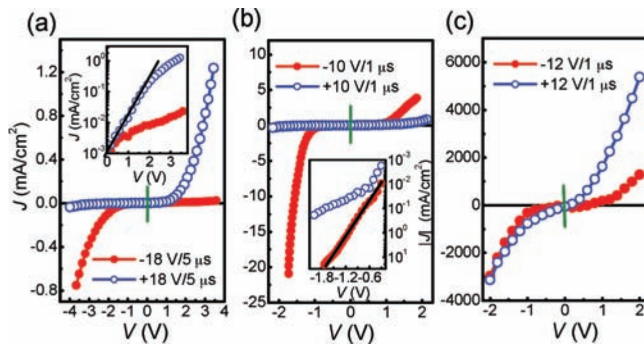

Figure 1. Diode-like bipolar conductance. Non-linear diode-like $J(V)$ curves for a) BFO1, b) BFO2–1, and c) BFO3 after applying poling pulses with different voltages and widths. Insets show one-side bias semilogarithmic scale plots, where the solid black lines indicate the voltage range for exponential J–V dependence.

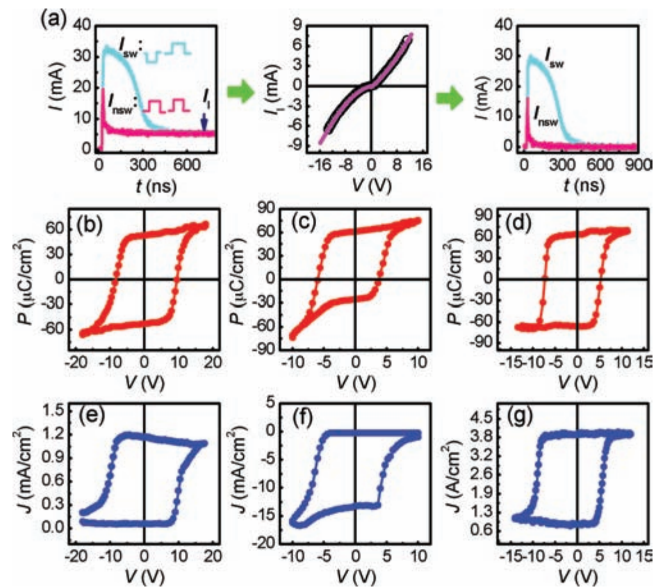

Figure 2. P–V hysteresis loops versus diode currents. a) The current transient $I(t)$ for BFO3 sampled by an oscilloscope from (–10 V, +10 V) or (+10 V, +10 V) pulse sequence consists of two currents of $I_{sw}(t)$ and $I_l(t)$ or $I_{nsw}(t)$ and $I_l(t)$ in the left panel. The $I_l(V)$ function is defined from the least-squares cubic polynomial fit of the I_l–V dependence shown by the solid line in the middle panel. $I_{sw}(t)$ and $I_{nsw}(t)$ are thus independently separated from $I(t)$, as shown in the right panel. After time integrations of the displacement currents under different V, we obtain P–V hysteresis loops for b) BFO1, c) BFO2–1, and d) BFO3 in comparison with their hysteretic current loops in e–g) at fixed reading voltages of 4.0, –2.0, and 2.0 V, respectively, after each pulse voltage in P–V loops.

lower electrode was grounded), the current density versus small voltage (J–V) curve exhibits diode-like conduction, i.e., the current along the poling direction is much higher than the reverse current, as shown in **Figure 1**a. Switching of the poling direction to –18 V results in a reversal of the current rectification direction, and the on/off current ratio exceeds 100 at 4 V, as seen clearly from the inset. A film thickness decrease from 500 to 240 nm increases the diode current density of BFO2–1 at negative bias by more than an order of magnitude (Figure 1b). The semilogarithmic scale inset in Figure 1b shows that the current is of the same order of magnitude in BFO bulk crystals with a large on/off current ratio.[3] However, the diode effect disappears at positive bias. The further reduction of the film thickness to 120 nm (BFO2–2) can enhance the negative diode current significantly, but an electrical damage of the capacitor is immediately involved at a poling voltage of 5 V (data not shown).

An increase in O_2 pressure from 10 to 30 Pa during film growth can result in an increase of more than two orders of magnitude in the forward current density at 2.0 V on BFO3 after a poling pulse of 12 V, though the on/off current ratio drops rapidly to 4.2:1, as shown in Figure 1c. This current density supplies a sufficient read current of 0.54 nA in a capacitor-type cell size of 100 nm.

Smearing of the diode effect on one side of the voltage axis in Figure 1b,c was attributed to the film thickness reduction that promotes preferential domain orientations in the as-grown state.[12,21] To measure the preferred polarization, most commercial ferroelectric testers that adopt a virtual-ground measuring system cannot discriminate between ferroelectric displacement and leakage charges. Therefore, we adopted a different procedure of short-pulse characterization to separate the two charges, modified from the positive-up-negative-down (PUND) technique originally used by Scott et al.[22] The total transient current I with time t under a step-like input voltage pulse of $V_{in}(t)$ across a ferroelectric capacitor C_f is monitored by an oscilloscope through an in-series resistor of $R_L = 100\ \Omega$ (Supporting Information, Figure S2a). After the first presetting pulse of –10 V or +10 V on BFO3, we observed the domain switching or non-switching current transient of $I_{sw}(t)$ or $I_{nsw}(t)$ overlapping the leakage current at +10 V, as shown in **Figure 2**a (the left panel). After completion of domain switching, $I(t)$ attenuates at a leakage current level I_l with the stable voltage across the ferroelectric at $V = V_{in} - R_l I_l$. Using a least-squares cubic polynomial fit of the I_l–V dependence, as shown by the solid line in the central part of Figure 2a, we obtain a coefficient for each polynomial term. From this defined $I_l(V)$ polynomial function and relationship $V(t) = V_{in}(t) - I(t)R_l$, where $I(t) = I_{sw}(t)$ (or $I_{nsw}(t)$) + $I_l(t)$, we can calculate $I_l(V(t))$. After subtraction of $I_l(V(t))$ from $I(t)$, we obtain $I_{sw}(t)$ or $I_{nsw}(t)$, as shown in right most part of Figure 2a, and the two current integrations over time correspond to switching and nonswitching polarization charges of $P_{sw}S$ and $P_{nsw}S$, where S is the electrode area.

From the step-by-step increase in V of the above pulse, we obtained two P_{sw}–V and P_{nsw}–V dependencies with respect to positive and negative presetting voltages. After centralization of the two dependencies along the P-axis, we derived P–V hysteresis loops, as shown in Figure 2b–d for BFO1, BFO2–1, and BFO3, respectively. The loops are almost symmetric for BFO1 and BFO3 with the remanent polarization $P_r \approx 60\ \mu C\ cm^{-2}$, coincident with the (001)-oriented BFO bulk crystal.[23] However, an asymmetric loop appears in BFO2–1 (Figure 2c), which implies a perceptible back-switching of the domains pointing to the lower electrode upon a voltage increase from –10 to –5 V. This back-switching enlarges the off current considerably at positive reading bias in Figure 1b and smears the diode effect along this direction. Consequently, the currents are read at

© 2011 WILEY-VCH Verlag GmbH & Co. KGaA, Weinheim

fixed voltages of 4.0, –2.0, and 2.0 V for BFO1, BFO2–1, and BFO3, respectively, after each voltage pulse in their *P–V* hysteresis loops.

Figure 2e–g shows the hysteretic resistive switching of the diodes, which have identical shapes to the *P–V* loops in Figure 2b–d, clearly indicating hysteretic modulation of the diode current by the ferroelectric polarization. This is the first clear evidence of a ferroresistive switching mechanism in capacitor-type multiferroic BFO thin films, which is completely different from the electromigration of oxygen vacancies or repetitive creation and rupture of electrical conductive paths in other resistive switching materials.[24,25]

To clarify the one-side diode effect in Figure 1b,c, we measured the time dependence of the switched domains preferentially pointing to the upper or lower electrode under a sequence of positive–negative or negative–positive pulses separated by *t*, as shown in **Figure 3**a–c. The volume fractions of the preferential domains pointing to the upper versus lower electrode (the as- grown state) after a relaxation time of 1 s are estimated as 5.5 versus 7.7% for BFO1, 4.0 versus 38% for BFO2–1, and 10 versus 13% for BFO3. Even a small fraction of domain back-switching into a reading field direction would enhance the off current by orders of magnitude, especially for BFO3 in Figure 1c. Nevertheless, the reversed domains are at a minimum in the thickest film of BFO1 with sufficient relaxation of epitaxial stresses.

The AFM images in **Figure 4**a shows that BFO2–2 possesses plate-like growth grains. The domain back-switching can be observed from the piezoelectric phase imaging of domain patterns in a microscopic scale after applying the poling voltages of +/–8 V through the tip scanning of piezoresponse force microscopy (PFM) on the film surface, as shown in Figure 4b. As expected, the negatively polarized region shows the discernible

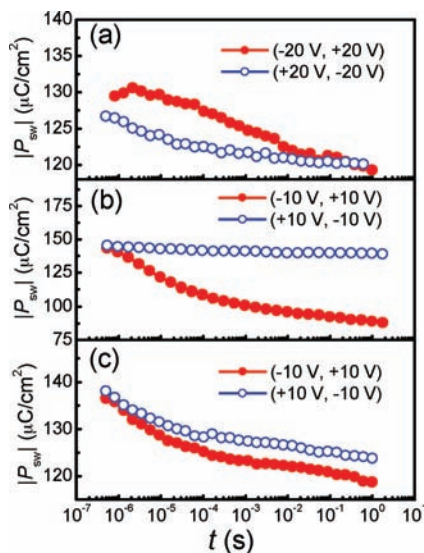

Figure 3. Time dependence of preferential domain polarization. The switched domain fraction versus time in the as-grown state is analyzed for a) BFO1, b) BFO2–1, and c) BFO3 through $P_{sw}(t)$ measurements under a positive–negative/negative–positive pulse sequence with widths of 2.5, 0.5, and 1.0 μs, respectively. *t* is the relaxation time between the two opposite pulses.

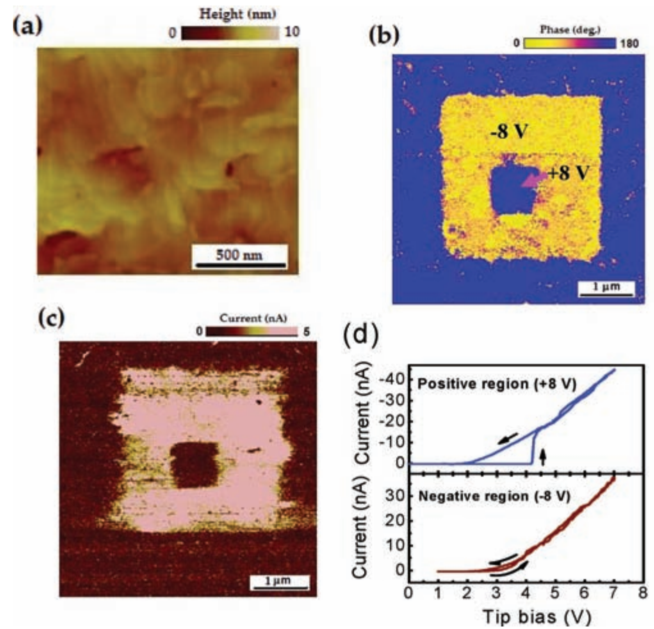

Figure 4. Local polarization and diode current for BFO2–2. a) AFM image of the film topography. b) Piezoelectric phase image of original preferred polarization patterns (downward) switched upward through PFM tip scanning of the film surface at –8 V within a square area of 3 × 3 μm². After that, the polarization in the center 1 × 1 μm² area is scanned downward at +8 V. c) The diode current mapping at –3 V acquired in the same region as in (b). d) The forward and backward voltage sweeping of the diode current within the positively and negatively polarized regions in (b).

domain back-switching into the preferred as-grown domain state pointing to the lower electrode, in contrast to the uniformly distributed domains within the positively polarized region. The high current contrast of the two regions mapped at –3 V in current conductive AFM mode matches the PFM domain patterns, as shown in Figure 4c. An abrupt jump of a small current into a high current occurs at –4.2 V in Figure 4d (the upper bound) due to domain switching during a negative voltage sweep from 0 to –7 V within a positively polarized region, which nevertheless disappears from the region oppositely polarized (the lower bound). The estimated diode current density is over 5 orders of magnitude higher than that reported by Blom et al.[2]

The reduction in film thickness and enhancement in deposition ambient O_2 pressure change the film growth habits and epitaxial stresses (Supporting Information, Figure S1d). The plate-like BFO2–2 grains in Figure 4a change into big islands with a much rougher film surface in releasing epitaxial stresses[19] as the film thickness is increased from 120 to 240 nm and above (BFO2–1 and BFO1), as confirmed from the AFM analysis (Supporting Information, Figure S3a,b). However, with enhancement of the deposition pressure from 10 to 30 Pa, the island growth mode in BFO2–1 returns to the plate-like growth in BFO3 (Supporting Information, Figure S3c), which exhibits a large diode current. The consequent O_2 annealing of the samples at 500 °C for 8 h reduced the diode current by more than two orders of magnitude (Supporting Information, Figure S6).

Physical understanding of the semiconducting behavior in the unintentionally doped wide-bandgap BFO films arises from

© 2011 WILEY-VCH Verlag GmbH & Co. KGaA, Weinheim

the possible existing oxygen deficiencies, as confirmed from the O_2 annealing experiment. According to Yuan and Wang's model,[26] the oxygen vacancy acting as donors can release one or two electrons to neutralize the positive boundary charge of domains to bend the band downward. This carrier accumulated region has a very small thickness and works as a quasi-ohmic contact with the electrode. On the other hand, the positively charged oxygen vacancies near the negative boundary charge at the opposite end bend the band upward, which constitutes a Schottky-type metal-semiconducting ferroelectric contact showing rectifying diode characteristics. The built-in internal field near the Schottky-type contact is directed from the positive to the negative bound charge and alters its direction upon polarization reversal. Therefore, the diode forward current antiparallel to the internal field increases exponentially with the voltage, as indicated by the black solid lines in the insets of Figure 1a,b. The ferroelectric bound charges are not supposed to be compensated completely by the electrode charges due to the interfacial effect.[27] The asymmetric configuration of the electrode (Pt and SRO) may induce different degrees of compensation of ferroelectric bound charges at the two interfaces and even a stationary internal field due to the work function mismatch. However, a qualitative model for the asymmetric interface of the metal–ferroelectric–metal structure is not altered by this factor,[3,26] in agreement with our experimental determination using symmetric SRO upper electrodes (data not shown). The change in grain growth habit between BFO2–1 and BFO3 may alter the film interfacial layers and thus their diode current.[5]

The bistable conductance in the diode can be non-destructively accessed in an arbitrarily long amount of time. **Figure 5**a shows extended retention in BFO2–1 read at –2.0 V unipolar pulse. Within the experimental time interval (≈1 month), both on and off currents vary little with time. The excellent retention stems from the intrinsic non-volatile nature of spontaneous switching and nonswitching polarization (P_{sw} and P_{nsw}). Under bipolar switching of the domains at ±10 V, $2P_r$ initially increases with the fatigue number N, suggesting depinning of the preferred domains. Thereafter, the film is susceptible to polarization fatigue, as shown in Figure 5b, and becomes much leakier. The separated fatigue leakage current is unable to be modulated by the poling field due to the nearby pinned domains (Supporting Information, Figure S4a–c show this current separation and dependence on N), unlike the diode current $J_{diode}(N)$, which is defined as the difference between on and off current densities. The shape for $J_{diode}(N)$ matches the $2P_r(N)$ profile, as shown in Figure 5b, which were also observed in BFO1 and BFO3 (Supporting Information, Figure S4a–c and Figure S5a,b), implying their intimate correlation. The solid lines in Figure 5b are the lines of best fit of the data using a domain pinning and depinning model.[28] Microscopically, the fatigued regions within the film have randomly distributed conductive domain walls[29] and defect aggregations,[30] which both offer high leakage paths.

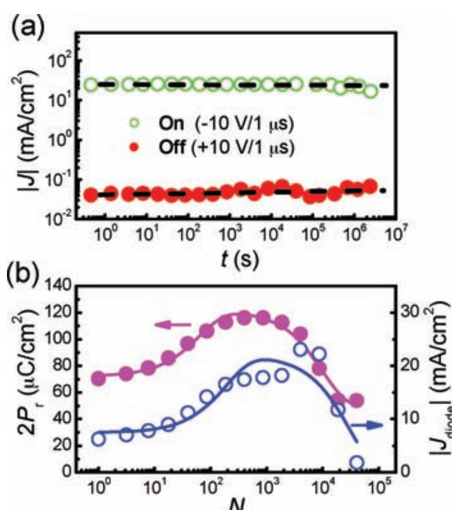

Figure 5. On/off current retention and polarization fatigue in BFO2–1. a) Time dependence of absolute on/off current densities in BFO2–1 read at –2 V after two opposite writing pulses. b) $2P_r$ – N and $|J_{diode}|$ – N dependence under fatigue pulses with voltage/width of 10 V/1.0 µs read at –2.0 V. The two solid lines best fit the data according to the fatigue model (Supporting Information, Figure S4a–c).

In summary, we have reported bistable diode currents up to 5.4 A cm^{-2} in Pt/$BiFeO_3$/$SrRuO_3$ thin-film capacitors through a change in polarization direction. The extracted P–V hysteresis loop from pulse-type polarization measurements matches the shape of the hysteretic on/off currents read after different polarization pulses. The ferroresistive nature of BFO semiconductors, eliminating the requirement of ultrathin and low-yield tunneling ferroelectric film, greatly facilitates nanoscale memory device fabrication. It was clearly demonstrated that ferroelectricity and conductivity coexist in a single phase, and the conductivity was modulated by ferroelectricity. A high diode current in $BiFeO_3$ with a plate-like growth mode is supposedly ubiquitous in other ferroelectric semiconductors. A multiferroic nature of this kind of materials may additionally permit the magnetic writing and electrical non-destructive readout of a multifunctional memory. These properties facilitate the advanced design of switchable devices combing spintronic, electronic, and optical functionalities.

Experimental Section

$BiFeO_3$ thin films were deposited on (100) $SrTiO_3$ single-crystal substrates at 650 °C using pulsed laser deposition. During deposition, the flowing oxygen pressure was between 10 and 30 Pa, and the pulsed KrF excimer laser beam (wavelength 248 nm) was focused to reach a laser fluence of 1–2 J cm^{-2} on the ceramic target surface. For electrical measurements, the 150-nm-thick epitaxial $SrRuO_3$ (SRO) conductive layer was pregrown as a lower electrode. The crystal structures were investigated by X-ray diffraction (Bruker X-ray Diffractometer D8) with Cu $K_{\alpha 1}$ radiation. Both low-magnification and high-resolution cross-sectional transmission electron microscopy (TEM) images were recorded on $BiFeO_3$ films using a JEOL-2010 analytical electron microscope. The film thickness was characterized using a GES5E spectroscopic ellipsometer. The film surfaces were studied with a Veeco MultiMode-V AFM operated in tapping mode, with combination techniques for the nanoscale polarization detection PFM (using Pt-coated silicon cantilever at an ac voltage of 250 kHz with an amplitude of 1 V) and spatially resolved conductance measurements in the current conductive AFM mode (using Si tips coated with B-doped diamond) with a scanning rate of 1.0 Hz.

The upper circular Pt electrodes (8.5×10^{-5}–5.0×10^{-4} cm^2) were deposited on the films at 500 °C through a shadow mask using ULVAC

© 2011 WILEY-VCH Verlag GmbH & Co. KGaA, Weinheim

ACS-4000-C4 magnetron sputtering. The input domain switching pulse was supplied by an Agilent 81150A waveform generator with a rise time of 7.5 ns, and the switching current was monitored through an in-series LC WR 6200A oscilloscope with the internal resistance of either 50 Ω or 1 MΩ.

Supporting Information

Supporting Information is available from the Wiley Online Library or from the author.

Acknowledgements

The authors thank M. C. Chen for the AFM, PFM, and C-AFM performance. This work was funded by the National Natural Science Foundation of China (10874226), the National Basic Research Program of China, Shanghai Key Program (1052nm07600), and the Program for Professor of Special Appointment (Eastern Scholar) at Shanghai. C.S.H appreciates the support from the Converging Research Center Program (2009–0081961) and the World Class University program (R31–2008-000–10075-0) through the National Research Foundation of Korea funded by the Ministry of Education, Science and Technology. A.Q.J. and C.W. contributed equally to this work.

Received: November 23, 2010
Published online: January 31, 2011

[1] J. F. Scott, *Ferroelectric Memories*, Springer, Heidelberg, Germany **2000**.
[2] P. W. M. Blom, R. M. Wolf, J. F. M. Cillessen, M. P. C. M. Krijn, *Phys. Rev. Lett.* **1994**, *73*, 2107.
[3] T. Choi, S. Lee, Y. J. Choi, V. Kiryukhin, S. W. Cheong, *Science* **2009**, *324*, 63.
[4] L. Pintilie, V. Stancu, L. Trupina, I. Pintilie, *Phys. Rev. B* **2010**, *82,* 085319.
[5] L. Pintilie, I. Vrejoiu, D. Hesse, G. LeRhun, M. Alexe, *Phys. Rev. B* **2007**, *75*, 104103.
[6] D. S. Rana, I. Kawayama, K. Mavani, K. Takahashi, H. Murakami, M. Tonouchi, *Adv. Mater.* **2009**, *21*, 2881.
[7] M. Dawber, J. F. Scott, unpublished.
[8] M. Y. Zhuravlev, R. F. Sabirianov, S. S. Jaswal, E. Y. Tsymbal, *Phys. Rev. Lett.* **2005**, *94*, 246802.
[9] P. Maksymovych, S. Jesse, P. Yu, R. Ramesh, A. P. Baddorf, S. V. Kalinin, *Science* **2009**, *324*, 1421.
[10] A. Gruverman, D. Wu, H. Lu, Y. Wang, H. W. Jang, C. M. Folkman, M. Y. Zhuravlev, D. Felker, M. Rzchowski, C. B. Eom, E. Y. Tsymbal, *Nano Lett.* **2009**, *9*, 3539.
[11] V. Garcia, S. Fusil, K. Bouzehouane, S. Enouz-Vedrenne, N. D. Mathur, A. Barthelemy, M. Bibes, *Nature* **2009**, *460*, 81.
[12] C. S. Ganpule, A. L. Roytburd, V. Nagarajan, B. K. Hill, S. B. Ogale, E. D. Williams, R. Ramesh, J. F. Scott, *Phys. Rev. B.* **2001**, *65*, 014101.
[13] A. Beck, J. G. Bednorz, C. Gerber, C. Rossel, D. Widmer, *Appl. Phys. Lett.* **2000**, *77*, 139.
[14] S. F. Karg, G. I. Meijer, J. G. Bednorz, *IBM J. Res. Dev.* **2008**, *52*, 481.
[15] R. Waser, M. Aono, *Nat. Mater.* **2007**, *6*, 833.
[16] J. J. Yang, M. D. Pickett, X. M. Li, D. A. A. Ohlberg, D. R. Stewart, R. S. Williams, *Nat. Nanotechnol.* **2008**, *3*, 429.
[17] A. Sawa, *Mater. Today* **2008**, *11*, 28.
[18] T. Zhao, A. Scholl, F. Zavaliche, K. Lee, M. Barry, A. Doran, M. P. Cruz, Y. H. Chu, C. Ederer, N. A. Spaldin, R. R. Das, D. M. Kim, S. H. Baek, C. B. Eom, R. Ramesh, *Nat. Mater.* **2006**, *5*, 823.
[19] H. W. Jang, D. Ortiz, S. H. Baek, C. M. Folkman, R. R. Das, P. Shafer, Y. Chen, C. T. Nelson, X. Pan, R. Ramesh, C. B. Eom, *Adv. Mater.* **2009**, *21*, 817.
[20] H. Zheng, J. Wang, S. E. Lofland, Z. Ma, L. Mohaddes-Ardabili, T. Zhao, L. Slamanca, S. R. Shinde, S. B. Ogale, F. Bai, D. Viehland, Y. Jia, D. G. Schlom, M. Wuttig, A. Roytburd, R. Ramesh, *Science* **2004**, *303*, 661.
[21] V. Nagarajan, S. Prasertchoung, T. Zhao, H. Zheng, J. Ouyang, R. Ramesh, W. Tian, X. Q. Pan, D. M. Kim, C. B. Eom, H. Kohlstedt, R. Waser, *Appl. Phys. Lett.* **2004**, *84*, 5225.
[22] J. F. Scott, L. Kammerdiner, M. Parris, S. Traynor, V. Ottenbacher, A. Shawabker, W. F. Oliver, *J. Appl. Phys.* **1988**, *64*, 787.
[23] D. Lebeugle, D. Colson, A. Forget, M. Viret, P. Bonville, J. F. Marucco, S. Fusil, *Phys. Rev. B* **2007**, *76*, 024116.
[24] D. H. Kwon, K. M. Kim, J. H. Jang, J. M. Jeon, M. H. Lee, G. H. Kim, X. S. Li, G. S. Park, B. Lee, S. Han, M. Kim, C. S. Hwang, *Nat. Nanotechnol.* **2010**, *5*, 148.
[25] C. H. Yang, J. Seidel, S. Y. Kim, P. B. Rossen, P. Yu, M. Gajek, Y. H. Chu, L. W. Martin, M. B. Holcomb, Q. He, P. Maksymovych, N. Balke, S. V. Kalinin, A. P. Baddorf, S. R. Basu, M. L. Scullin, R. Ramesh, *Nat. Mater.* **2009**, *8*, 485.
[26] G. L. Yuan, J. Wang, *Appl. Phys. Lett.* **2009**, *95*, 252904.
[27] M. Stengel, D. Vanderbilt, N. A. Spaldin, *Nat. Mater.* **2009**, *8*, 392.
[28] A. Q. Jiang, Y. Y. Lin, T. A. Tang, *Appl. Phys. Lett.* **2006**, *89*, 032906.
[29] J. Seidel, L. W. Martin, Q. He, Q. Zhan, Y. H. Chu, A. Rother, M. E. Hawkridge, P. Maksymovych, P. Yu, M. Gajek, N. Balke, S. V. Kalinin, S. Gemming, F. Wang, G. Catalan, J. F. Scott, N. A. Spaldin, J. Orenstein, R. Ramesh, *Nat. Mater.* **2009**, *8*, 229.
[30] E. L. Colla, I. Stolichnov, P. E. Bradely, N. Setter, *Appl. Phys. Lett.* **2003**, *82*, 1604.

© 2011 WILEY-VCH Verlag GmbH & Co. KGaA, Weinheim